Infrared Physics & Technology 54 (2011) 302–305

Contents lists available at ScienceDirect

Infrared Physics & Technology

journal homepage: www.elsevier.com/locate/infrared

Terahertz and infrared detectors based on graphene structures

Victor Ryzhii [a,b,*], Maxim Ryzhii [a,b], Nadezhda Ryabova [a,b], Vladimir Mitin [c], Taiichi Otsuji [b,d]

[a] Computational Nanoelectronics Laboratory, University of Aizu, Aizu-Wakamatsu 965-8580, Japan
[b] Japan Science and Technology Agency, CREST, Tokyo 107-0075, Japan
[c] Department of Electrical Engineering, University at Buffalo, Buffalo, NY 14260, USA
[d] Research Institute of Electrical Communication, Tohoku University, Sendai 980-8577, Japan

ARTICLE INFO

Article history:
Available online 27 December 2010

Keywords:
Detector
Graphene
Photocurrent
Dark current
Responsivity
Detectivity

ABSTRACT

We consider newly proposed terahertz and infrared interband detectors based on multiple-graphene-layer structures with p–i–n junctions. Using the developed device model, we calculate the photodetector characteristics (responsivity and dark current limited detectivity) and compare them with the characteristics of other photodetectors. It is shown that due to relatively high quantum efficiency and weakened thermogeneration processes, the detectors under consideration can exhibit superior performance.

1. Introduction

Carbon structures based on monolayers of carbon atoms forming a dense honeycomb two-dimensional crystals, namely, graphite, individual graphene layers (GLs), and graphene bilayers (GBLs) exhibit quite different electron and optical characteristics. Unique properties of GLs and GBLs [1,2] make them promising for different nanoelectronic and optoelectronic device applications. The gapless energy spectrum of GLs, which is an obstacle for creating transistor-based digital circuits, promotes the use of GLs in terahertz (THz) and infrared (IR) devices. The possibility of the opening of the energy gap in GBLs by applying the transverse electric field also can be useful in the device application. The discovery of the fact (see Ref. [3] and the references therein) that the multiple GL structures with disoriented stacks of GLs (with the non-Bernal stacking) exhibit the same energy spectrum as an individual GL, opens up an opportunity of creating effective THz and IR lasers and detectors based on such structures [4,5]. The main advantage of the disoriented multiple-GL structure in comparison with the single GL structure is much higher interband quantum efficiency (which increases with increasing number of GLs in the structure). Due to high quantum efficiency as well as features of their absorption spectrum and thermogeneration processes, THz and IR photodetectors based on GL structures can occupy a marked place among other well documented photodetectors [6–10], particularly considering a very fast progress in graphene industrial production techniques [11].

In this paper, we consider the characteristics of THz and IR interband detectors based on multiple GL structures with the p–i–n junctions extending our previous publication [5], in particular, including the examination of the role of interband tunneling at lowered temperatures. The devices under consideration are shown in Fig. 1. The p–i–n junctions in these multiple-GL photodiodes (MGL-PDs) can be formed due to a chemical doping [12]. These junctions in the gated multiple GL structures with not to many GLs can also be electrically induced [5,13] (as in individual GLs [14]). Our consideration is primarily focused on MGL-PDs with chemically doped n- and p-sections. The MGL-PDs with “electrical doping” can be treated similarly (with limited number of GLs). We compare the characteristics of MGL-PDs with those of some other photodetectors, particularly, with GBL field-effect phototransistors (GBL-PTs) with n–p–n junctions proposed recently [15].

2. Characteristics of GL-PDs

We consider the MGL-PDs with the structures shown in Fig. 1(a) and (b) under the reverse bias voltage V assuming their irradiation by normally incident THz/IR radiation with the intensity I and frequency Ω. The p- and n-sections in the structure in Fig. 1(b) are formed due to the gate voltages V_p and V_n. Due to the reverse voltage bias, depleted i-sections are formed in each GL between the p- and n-sections adjacent to the pertinent side contacts. As in the customary p–i–n photodiodes, the electrons and holes

* Corresponding author at: Computational Nanoelectronics Laboratory, University of Aizu, Aizu-Wakamatsu 965-8580, Japan.
E-mail address: v-ryzhii@u-aizu.ac.jp (V. Ryzhii).

1350-4495/$ - see front matter © 2010 Elsevier B.V. All rights reserved.
doi:10.1016/j.infrared.2010.12.034

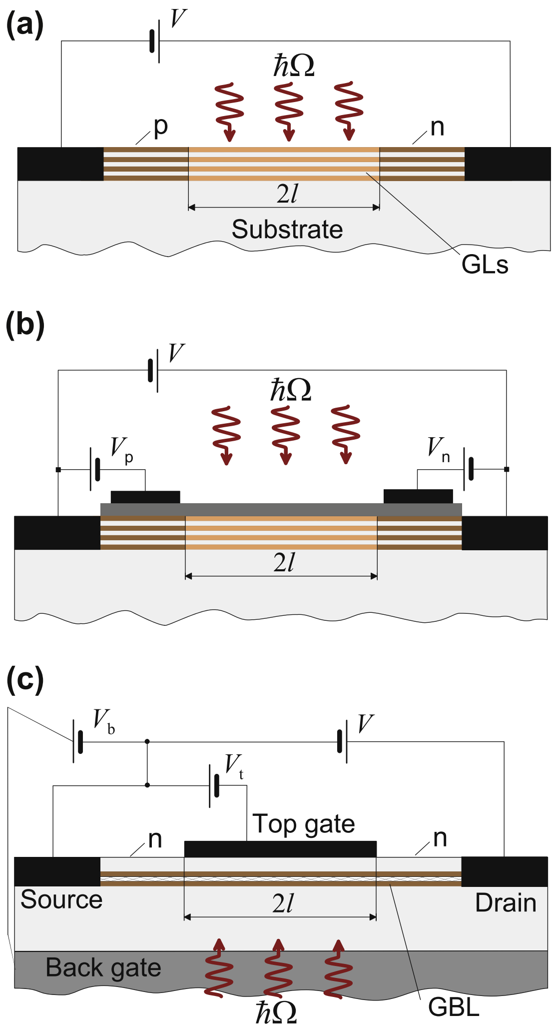

Fig. 1. Schematic views of MGL-PDs with (a) chemically doped *p*- and *n*-regions, (b) with electrically-induced *p*–*i*–*n* junction, and (c) GBL-PT with electrically induced *n*–*p*–*n* junction.

photogenerated in the *i*-sections induce the terminal current which constitutes the output electric signal. Disregarding the recombination of electrons and holes in the *i*-sections of all GLs, the net photocurrent (per unit width perpendicular perpendicular to its direction) can be presented as

$$J_{photo} = \frac{4le[1-(1-\beta_\Omega)^K)]}{\hbar\Omega} I. \tag{1}$$

Here, e is the electron charge, $2l$ is the length of the *i*-sections (see Fig. 1), $\hbar$ is the reduced Planck constant, K is the number of GLs, and β_Ω is the interband absorption coefficient of radiation. The latter is given by Falkovsky and Varlamov [16]

$$\beta_\Omega = \beta[1 - F(\hbar\Omega/2)], \tag{2}$$

where $\beta = \pi e^2/c\hbar \simeq \pi/137 \simeq 0.023$, c is the speed of light in vacuum, and $F(\varepsilon)$ is the electron (hole) energy distribution function in the *i*-sections of each GL. At moderate irradiation and reverse bias conditions, the electron and hole densities in the *i*-sections are much smaller that the equilibrium density (at which $F_{th}(0) = 1/2$). Hence, strongly nonequilibrium conditions under consideration, $F(\hbar\Omega/2) < F(0) \ll 1/2$. Due to this, the term with $F(\hbar\Omega/2)$ in Eq. (2) can be neglected (see also below). As a result, using Eqs. (1) and (2), the MGL-PD responsivity can be presented in the following form:

$$R = \frac{2e[1-(1-\beta_\Omega)^K]}{\hbar\Omega} \simeq K^* \frac{2e\beta}{\hbar\Omega} = \frac{e\eta}{\hbar\Omega}, \tag{3}$$

where $K^* = [1-(1-\beta)^K)]/\beta$. The quantity $\eta = 2[1-(1-\beta)^K)] = 2\beta K^*$ constitutes the MGL-PD quantum efficiency. If $K = 20$, one obtains $\eta \simeq 74\%$, while at $K = 1$, $\eta \simeq 4.6\%$ The dependences of the MGL-PD responsivity R on the number of GLs K calculated for different radiation frequencies $f = \Omega/2\pi$ are shown in Fig. 2. One can see that the responsivity of MGL-PDs with sufficiently large number of GLs is very high in fairly wide range of radiation frequencies. This is attributed to a strong interband absorption (in each of the multiple GLs) and almost flat its spectral dependence.

The dark current, J_{dark}, in MGL-PDs is determined by the rates of thermogeneration and interband tunneling, g_{th} and g_{tunn}:

$$J_{dark} = 4Kel(g_{th} + g_{tunn}). \tag{4}$$

The dark-current limited detectivity, D^*, can be expressed in term of the responsivity, R and the dark current, J_{dark}, as

$$D^* = R\sqrt{\frac{A}{4eJ_{dark}}H}, \tag{5}$$

where $A = 2lH$ is the GL-PD area and H is the detector width in the direction perpendicular to the current. Eqs. (3)–(5) yield

$$D^* = \frac{K^*\beta}{\sqrt{2K(g_{th} + g_{tunn})}\hbar\Omega}. \tag{6}$$

To achieve maximum detectivity at chosen temperature, one needs to suppress the tunneling current up to the acceptable level. The tunneling current is proportional to $V^{3/2}/\sqrt{l}$ [5,17]. Hence at sufficiently low bias voltages in the MGL-PDs with not too short *i*-sections at elevated temperatures, the detectivity limited by the thermogeneration. Fig. 3 shows the D^* versus K dependences calculated using Eq. (6) for different radiation frequencies $f = \Omega/2\pi$. For the calculations, the values of the thermogeneration rate were assumed those calculated previously: $g_{th} = 10^{21}\ \mathrm{cm^{-2}\,s^{-1}}$ at $T = 300$ K and $g_{th} = 10^{13}\ \mathrm{cm^{-2}\,s^{-1}}$ at $T = 77$ K, respectively [18].

One of the most important points, which follows from Fig. 3, is fairly high values of the detectivity at room temperatures.

In Eq. (2), we neglected the dependence of the interband absorption coefficient β_Ω on $F(\hbar\Omega/2)$, i.e., on the population of the conductance and valence bands at nonequilibrium conditions under consideration. This is justified if $F(0)$ is small. The latter quantity can be estimated as $F(0) = 2g_{th}l/\langle v\ \rangle\Sigma_{th}$, where Σ_{th} is the equilibrium electron and hole density and $\langle v\rangle$ is the mean electron and hole velocity in the *i*-sections. This velocity varies from $\langle v\ \rangle \simeq v_W/2$, in the ballistic regime to $\langle v\rangle \simeq \mu V/2l$ in the case of the transport of electrons and holes controlled by their scattering ($v_W = 10^8$ cm/s is the characteristic velocity in GLs [1,2] and μ is the electron and hole mobility). Setting $2l = 30\ \mu$m, $\langle v\rangle = 5 \times 10^7$ cm/s, $g_{th} = 10^{13}\ \mathrm{cm^{-2}\,s^{-1}}$, and $\Sigma_{th} = 5.4 \times 10^9\ \mathrm{cm^{-2}}$ at $T = 77$ K we arrive at $F(0) \simeq 10^{-7}$. At $T = 300$ K, $\Sigma(0)$ is larger, but

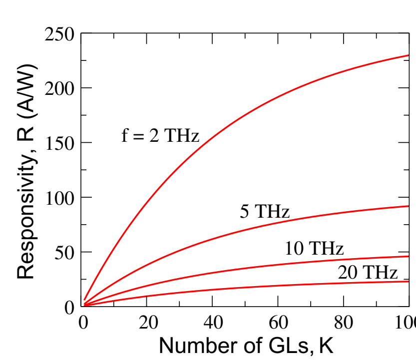

Fig. 2. Responsivity of MGL-PDs versus numbers of GLs for $f = \Omega/2\pi = 2 - 20$ THz.

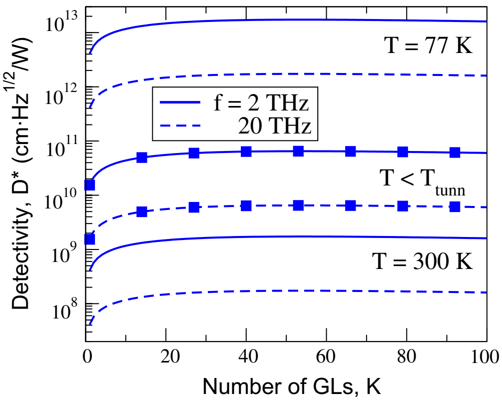

Fig. 3. Thermogeneration dark current limited detectivity of MGL-PDs versus numbers of GLs for $f = \Omega/2\pi = 2$ and 20 THz at $T = 300$ K and $T = 77$ K; markers indicate detectivity limited by tunneling dark current.

the value of $F(0)$ can also be sufficiently small due to the heating of electrons and holes by the electric field [19,20]. The inclusion of such a dependence leads to a weak dependence of β_Ω on Ω. The spectral dependence given by Eq. (2) can also be somewhat modified at low frequencies due to the collisional damping of the electron and hole spectra. However the incorporation of these effects requires a substantially more complex model.

3. Effect of tunneling

The interband tunneling in the i-section can markedly contribute to the dark current and decrease the MGL-PD detectivity. The rate of the tunneling in a GL at the electric field $\mathscr{E} = V/2l$ can be estimated as [17]

$$g_{tunn} = \frac{1}{4\pi v_W^{1/2}} \left(\frac{eV}{2l\hbar}\right)^{3/2}. \tag{7}$$

Using Eq. (7), one can arrive at the following condition, at which the tunneling weakly affects the detectivity ($g_{tunn} \ll g_{th}$):

$$\mathscr{E} = \frac{V}{2l} \ll (4\pi g_{th})^{2/3} \frac{\hbar v_W^{1/3}}{e} = \mathscr{E}_{tunn}. \tag{8}$$

The quantity $\mathscr{E}_{tunn}$ strongly depends on the temperature via the temperature dependence of g_{th}. Using the above data for g_{th}, for $T = 300$ K we obtain $\mathscr{E}_{tunn} \simeq 157$ V/cm. Assuming that the electron and hole mobility is $\mu = 4 \times 10^4$ cm^2 V^{-1} s^{-1} and setting $2l = 30$ μm, the pertinent transit time $t_{tunn} = 2l/\mu\mathscr{E}_{tunn} \simeq 5 \times 10^{-10}$ s. This time is of the same order of magnitude or shorter than the recombination time [18]. Hence, in MGL-PDs with such or shorter i-section, the role recombination is weak. In the samples with larger $2l$, the recombination can lead to a decrease in R and D^*.

At lower temperatures, the thermogeneration rate in GLs can be rather small, so that the main mechanism limiting the detectivity can be associated with the tunneling. The curves with markers in Fig. 3 correspond to the D^* vs K dependences calculated for the case of relatively low temperature at which the tunneling is the dominant mechanism of the dark current ($T < T_{tunn}$, where T_{tunn} is the temperature at which $g_{th} = g_{tunn}$ for a given strength of the electric field $\mathscr{E}$). It was assumed that $\mathscr{E} = 2.5$ V/cm. As it seen from comparison of the low-temperature dependences in Fig. 3, the tunneling dark current can substantially limit the detectivity. Rough estimates of the threshold temperature T_{tunn} (for $\mathscr{E} = 1.5$ V/cm) yield $T_{tunn} \sim 250$ K. Since at $T < T_{tunn}$ the electron and hole mobility can be fairly high and the ballistic transport along the i-section can occur, the transit time might be much shorter that the recombination time even at rather weak electric fields.

4. Comparison of MGL-PDs and GBL-PTs (quantum efficiency versus photoelectric gain)

Let us compare the characteristics of MGL-PDs with those of GBL-PTs. The structure of the latter which comprises a GBL is shown in Fig. 1(c). At positively biased back gate and negatively biased top gate, the GBL includes the n-section near the edge contacts and the p-section beneath the top gate, so that the n–p–n junction is formed [15]. In contrast to GLs, the energy spectrum of the GBL in the device in question exhibits the energy gap, $E_g \simeq ed(V_b - V_t)/2W$, i.e., proportional to the back- and top-gate voltages, V_b and V_t ($d \simeq 0.35$ nm is the spacing between GLs and W is the gate layers thickness). This leads to the voltage-controlled gap in the radiation absorption spectrum. Another feature is associated with the accumulation of the photogenerated holes under the top-gate. These holes affect the injection current between the side contact and provide the photoelectric gain. As follows from [15], at $\hbar\Omega \gtrsim E_g$, one can assume that the quantum efficiency in GBL-PTs is about β, i.e., much lower that in MGL-PDs with large K. For rough estimates, the thermogeneration rate in GBL-PTs can be assumed to be of the same order of magnitude as in MGL-PDs, despite the energy gap in the formers. This is because the thermogeneration at the temperatures of interest is associated by the absorption of optical phonons, whose energy $\hbar\omega_0 \simeq 0.2$ eV significantly exceeds the energy gap E_g. However, the photoelectric gain in GBL-PTs can be rather large [15]:

$$g_{GBL} \sim \exp\left[\frac{\varepsilon_F}{k_BT}\left(1 - \frac{4d}{a_B}\right)\right]. \tag{9}$$

Here, ε_F is the Fermi energy in the source contact, k_B is the Boltzmann constant and a_B is the Bohr radius. Setting $a_B = 4$ nm, for the term in the right-hand side of Eq. (7) one obtains $\exp(0.65\, \varepsilon_F/k_BT)$. Taking into account that the photoelectric gain in MGL-PDs is $g \simeq 1$ (electron-hole recombination in the i-sections of GLs is insignificant) and using simplified formulae from Ref. [15], for the ratios of R/R_{GBL} and D^*/D^*_{GBL} we obtain

$$\frac{R}{R_{GBL}} \simeq 2K^* \exp\left(-\frac{0.65\varepsilon_F}{k_BT}\right), \tag{10}$$

$$\frac{D^*}{D^*_{GBL}} \simeq \frac{2K^*}{\sqrt{K}} \exp\left(-\frac{0.325\varepsilon_F}{k_BT}\right)\sqrt{\frac{g_{th}}{(g_{th} + g_{th})}}. \tag{11}$$

In Eqs. (10) and (11), we omitted preexponential factors which are of the order on unity. We also have taken into account that the interband tunneling in the GBL-PTs is essentially suppressed due to the energy gap. The Fermi energy of electrons electrically induced near the source edge is equal to $\varepsilon_F \simeq eV_b(a_B/8W)$ [15]. Setting $W = 10$ nm and $V_b = 2$ V, we obtain $\varepsilon_F \simeq eV_b(a_B/8W) \simeq 100$ meV. In this case, assuming that $K = 20$ ($K^* \simeq 16$) at $T = 300$ K, we arrive at $R/R_{GBL} \simeq 2.4$ and $D^*/D^*_{GBL} \simeq 1.95$. At lower temperatures, this ratios can be smaller than unity. Indeed, for instance, at $T = 200$ K, $R/R_{GBL} \simeq 0.145$.

5. Comparison with some other photodetectors

Due to high interband absorption coefficient of GLs, which much higher than the intersubband absorption coefficient of quantum wells (QW) and quantum dot (QD) arrays, the responsivity of MGL-PDs (even with a small number of GLs) substantially exceeds that of QW infrared photodetectors (QWIPs), R_{QW}, and of QD infrared photodetectors (QWIPs), R_{QD} (whose responsivity is virtually independent of number of QL and QD arrays [7–9]). The MGL-PD detectivity also can be much higher than that of QWIPs and QDIPs due to both relatively high responsivity and lower thermogeneration rate [15]. Some increase in the ratios $R/R_{QW}, R/R_{QD}, D^*/D^*_{QW}$, and D^*/D^*_{QD} is possible when the probability of electron capture into QWs and QD arrays $p_c \ll 1$ (for more details see Ref. [5]).

As for comparison of MGL-PDs with the photodetectors based on narrow-gap and gapless bulk material akin to HgCdTe, the main possible advantage of the formers is lower thermogeneration rate. This is because the thermogeneration in GLs at not too low temperatures can be attributed to the absorption of optical phonons. However, due to very high optical phonon energy in GL ($\hbar\omega_0$ = 0.2 eV) compared to HgCdTe and other material, the probability of the optical phonon absorption in GLs accompanied by the interband transition is relatively small. In contrast to material like HgCdTe in which the Auger generation–recombination processes play an important role [10,21], such processes in GLs are forbidden [22].

6. Conclusions

Using the developed device model for MGL-PDs, we calculated their responsivity and detectivity and demonstrated that MGL-PDs with multiple GLs can exhibit the performance comparable with the performance of GBL-PTs. It is also shown that MGL-PDs can substantially surpass QWIPs and QDIPs.

Acknowledgement

The work was supported by the Japan Science and Technology Agency, CREST.

References

[1] K.S. Novoselov, A.K. Geim, S.V. Morozov, D. Jiang, M.I. Katsnelson, I.V. Grigorieva, S.V. Dubonos, A.A. Firsov, Two-dimensional gas of massless Dirac fermions in graphene, Nature 438 (2005) 197.
[2] A.H. Castro Neto, F. Guinea, N.M.R. Peres, K.S. Novoselov, A.K. Geim, The electronic properties of graphene, Rev. Mod. Phys. 81 (2009) 109.
[3] M. Orlita, M. Potemski, Dirac electronic states in graphene systems: optical spectroscopy studies, Semicond. Sci. Technol. 25 (2010) 063001.
[4] V. Ryzhii, M. Ryzhii, A. Satou, T. Otsuji, A.A. Dubinov, V. Ya. Aleshkin, Feasibility of terahertz lasing in optically pumped expitaxial multiple graphene laeyer structures, J. Appl. Phys. 106 (2009) 084507.
[5] V. Ryzhii, M. Ryzhii, V. Mitin, T. Otsuji, Terahertz and infrared photodetection using *p–i–n* multiple-graphene structures, J. Appl. Phys. 106 (2009) 084512.
[6] M. Razeghi (Ed.), Long Wavelength Infrared Detectors, Gordon and Breach, Amsterdam, 1996.
[7] K.K. Choi, The Physics of Quantum Well Infrared Photodetectors, World Scientific, Singapore, 1997.
[8] V. Ryzhii (Ed.), Intersubband Infared Photodetectors, World Scientific, Singapore, 2003.
[9] H. Schneider, H.C. Liu, Quantum Well Infrared Photodetectors, Springer, Berlin, 2007.
[10] A. Rogalski, Infrared Detectors, Taylor & Francis, 2009.
[11] M. Wilson, Graphene production goes industrial, Phys. Today (2010) 15.
[12] D. Farmer, Y.-M. Lin, A. Afzali-Ardakani, P. Avouris, Behavior of a chemically doped graphene junction, Appl. Phys. Lett. 94 (2009) 213106.
[13] M. Ryzhii, V. Ryzhii, V. Mitin, T. Otsuji, M.S. Shur, Electrically induced *n–i–p* junctions in multiple graphene layer structures, Phys. Rev. B 82 (2010) 075419.
[14] V.V. Cheianov, V.I. Fal'ko, Selective transmission of Dirac electrons and ballistic magnetoresistance of *n–p* junctions in graphene, Phys. Rev. B 74 (2006) 041403. R.
[15] V. Ryzhii, M. Ryzhii, Graphene bilayer field-effect phototransistor for Terahertz and infrared detection, Phys. Rev. B 79 (2009) 245311.
[16] L.A. Falkovsky, A.A. Varlamov, Space-time dispersion of graphene conductivity, Eur. Phys. J. B 56 (2007) 281.
[17] V. Ryzhii, M. Ryzhii, V. Mitin, M.S. Shur, Graphene tunneling transit-time terahertz oscillator based on electrically in duced *p–i–n* Junction, Appl. Phys. Express 2 (2009) 034503.
[18] F. Rana, P.A. George, J.H. Strait, S. Shivaraman, M. Chanrashekhar, M.G. Spencer, Carrier recombunation and generation rates for intravalley and intercalley phonon scattering in graphene, Phys. Rev. B 79 (2009) 115447.
[19] R.S. Shishir, D.K. Ferry, S.M. Goodnick, J. Phys. Conf. Ser. 193 (2009).
[20] O.G. Balev, F.T. Vasko, V. Ryzhii, Phys. Rev. B 79 (2009) 165432.
[21] A. Rogalski, J. Antoszewski, L. Faraone, Third generation infrared photodetector arrays, J. Appl. Phys. 105 (2009) 91101.
[22] M.S. Foster, I.L. Aleiner, Slow imbalance relaxation and thermoelectric transport in graphene, Phys. Rev.B 79 (2009) 85415.